RSC Advances

PAPER

View Article Online
View Journal | View Issue

Cite this: *RSC Adv.*, 2024, **14**, 26176

Bortezomib-encapsulated metal–phenolic nanoparticles for intracellular drug delivery†

Haidong Zhou, *[a] Hongyu Xu,[a] Jiaping Man[b] and Gangxiang Wang[a]

Bortezomib (BTZ) is an important boronate proteasome inhibitor that is widely used in cancer therapy. However, the clinical application of BTZ suffers from poor stability and serious adverse effects. Herein, we fabricated metal–polyphenol nanoparticles for the covalent encapsulation of BTZ. BTZ-encapsulated tannic acid (TA)–Fe^{3+} nanoparticles can be prepared by mixing BTZ, TA, and ferric chloride owing to the formation of metal–polyphenol coordination interaction and dynamic boronate ester bonds. The BTZ-encapsulated TA–Fe^{3+} nanoparticles (BTZ NPs) are stable in physiological environment (pH 7.4) with minimal drug leakage. However, BTZ NPs can be disassembled in an acidic environment. Therefore, BTZ can be rapidly released from BTZ NPs in an acidic environment (pH 5.0). More than 50% BTZ can be released from BTZ NPs after 8 h incubation at pH 5.0. BTZ NPs exhibited high cytotoxicity against human osteosarcoma Saos-2 cells and human multiple myeloma OPM-2 cells. The metal–polyphenol nanoparticles can be a promising nanoplatform for the delivery of BTZ with simultaneously enhanced therapeutic efficacy and reduced side effects.

Received 13th May 2024
Accepted 5th August 2024

DOI: 10.1039/d4ra03504f

rsc.li/rsc-advances

1. Introduction

Cancer is one of the most lethal diseases with very high morbidity and mortality.[1] Many chemotherapeutic agents, including doxorubicin, cisplatin, and gemcitabine, were developed to combat malignant tumors.[2] Bortezomib (BTZ) is the first FDA-approved boronic acid drug.[3] BTZ is a proteasome inhibitor, which exhibits antitumor activity by inhibiting the 26S proteasome, leading to the inhibition of the degradation of apoptosis-related proteins and subsequent programmed cancer cell death.[4] In clinic, BTZ is widely used in treating hematologic malignancies, including multiple myeloma and mantle cell lymphoma. Moreover, it was reported to be effective in treating bone tumors, such as osteosarcoma and osteoclastoma. However, the stability of BTZ is relatively poor during blood circulation due to its degradation by plasma proteases.[5] Meanwhile, the reactive boric acid groups of BTZ can chelate with plasma proteins, leading to the deactivation of BTZ.[6] BTZ exhibits serious side effects, including hematotoxicity, peripheral neurotoxicity, and myelosuppression.[7,8] These critical issues remarkably restrict the therapeutic efficacy of BTZ. The effectiveness of BTZ in treating solid tumors is even much worse due to nonspecific drug distribution and poor tumor penetration.[9,10] It is still a great challenge to achieve simultaneously enhanced therapeutic efficacy and reduced side effects of BTZ in cancer therapy.

Nanotechnology-based platform holds great promise in drug delivery, which promotes revolutionary advances in pharmaceutics.[11–15] For example, many nanoformulations such as Abraxane, Doxil, and DaunoXome were launched for cancer chemotherapy.[16,17] Drug-encapsulated nanoparticles show various advantages, including enhanced solubility, improved pharmacokinetics, targeting ability, and reduced side effects.[18–22] The fabrication of BTZ-encapsulated nanoparticles is a promising approach to achieve enhanced therapeutic efficacy and reduced side effects of BTZ simultaneously.[23–26] Therefore, various BTZ-encapsulated nanodelivery systems have been reported. For example, BTZ was physically encapsulated into BCMA antibody-functionalized poly(lactic-*co*-glycolic acid) (PLGA) nanoparticles for the targeted delivery of BTZ.[27] Taking advantage of the unique boric acid groups of BTZ, it can also be encapsulated into nanoparticles *via* covalent boronate–catechol linkages.[28,29] In a typical example, liposomal BTZ nanoparticles were prepared by the formation of boronate ester prodrugs, which significantly improved the therapeutic efficacy of BTZ *in vivo*.[30]

The formation of boronate–catechol linkages is a promising strategy to fabricate pH-sensitive BTZ-encapsulated nanoparticles. Polyphenols, which have the characteristic structures of multiple phenolic units, are ideal candidates to form polyphenol–BTZ complex *via* pH-sensitive boronate ester bonds. Moreover, polyphenols can coordinate with metal ions to form

[a]*Department of Orthopaedics, Shengzhou People's Hospital (Shengzhou Branch of the First Affiliated Hospital of Zhejiang University School of Medicine), 666 Dangui Road, Shengzhou, 312400, P. R. China. E-mail: 156035144@qq.com*

[b]*MOE Key Laboratory of Macromolecule Synthesis and Functionalization of Ministry of Education, Department of Polymer Science and Engineering, Zhejiang University, Hangzhou, 310058, P. R. China*

† Electronic supplementary information (ESI) available. See DOI: https://doi.org/10.1039/d4ra03504f

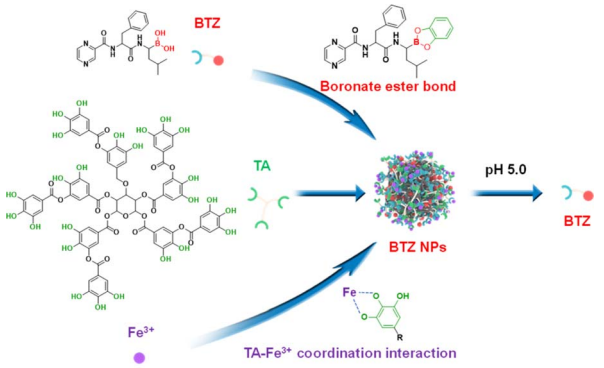

Scheme 1 Schematic illustration for the preparation of BTZ NPs by the self-assembly of BTZ, TA, and Fe^{3+}. The release of BTZ could be realized in an acidic environment.

metal–phenolic networks (MPN).[31–33] By controlling the assembly parameters, metal–polyphenol nanoparticles can be prepared.[34–37] Since the metal–polyphenol coordination interaction is pH-sensitive, the metal–polyphenol nanoparticles can be disassembled in an acidic microenvironment, which makes it possible to achieve pH-sensitive drug release.[38] Therefore, metal–polyphenol nanoparticles might be appropriate nanocarriers for the encapsulation of BTZ by the formation of pH-sensitive boronate–catechol linkages, although it has been rarely reported.

Herein, taking advantage of the pH-sensitive metal–polyphenol coordination self-assembly, we designed a BTZ-encapsulated metal–polyphenol nanoparticle for the delivery of BTZ (Scheme 1). BTZ can be assembled into Fe^{3+}–tannic acid (TA) nanoparticles by the formation of pH-sensitive boronate ester linkages. The BTZ-encapsulated TA–Fe^{3+} nanoparticles (BTZ NPs) are expected to be stable in physiological environment (pH 7.4) with minimal drug leakage. BTZ NPs can be disassembled in an acidic environment (pH 5.0) owing to the disruption of metal–polyphenol coordination self-assembly and cleavage of boronate ester linkages, leading to the efficient release of BTZ. BTZ NPs are confirmed to effectively inhibit the proliferation of cancer cells. The fabrication of BTZ NPs is expected to achieve simultaneously enhanced therapeutic efficacy and reduced side effects of BTZ in cancer therapy.

2. Experimental section

2.1 Materials

Bortezomib (BTZ, 98% purity) was purchased from Bidepharm Co., Ltd. (Shanghai, China). Tannic acid (TA, 95% purity) was bought from Aladdin Biochemical Technology Co., Ltd. (Shanghai, China). Anhydrous ferric chloride ($FeCl_3$, 97% purity) was supplied by Sinopharm Chemical Reagent Co., Ltd (Shanghai, China). Cell Counting Kit-8 (CCK-8) was purchased from BestBio Co., Ltd (Shanghai, China). Human umbilical vein endothelial cells (HUVEC), human multiple myeloma cell line OPM-2, and human osteosarcoma cell line Saos-2 were obtained from China Center for Type Culture Collection (CCTCC). All other chemical reagents were used as received without further purification.

2.2 Preparation of BTZ-encapsulated metal–polyphenol nanoparticles

TA and $FeCl_3$ were used to prepare metal–polyphenol nanoparticles in this research. Typically, 12.5 mg per mL BTZ in dimethyl sulfoxide (DMSO), 40 mg per mL TA aqueous solution, and 5 mg per mL $FeCl_3$ aqueous solution were prepared as stock solutions. 500 μL of BTZ solution, 500 μL of TA solution, and 50 μL of $FeCl_3$ solution were added into 10 mL ultrapure water. The mixture was stirred for 2 h (800 rpm). After that, the mixture was centrifuged at 8000 rpm for 3 min. The precipitate was collected and re-dispersed in 10 mL ultrapure water. Finally, the suspension was centrifuged again at 8000 rpm for 3 min. The precipitate was collected and re-dispersed in ultrapure water, which was stored at 4 °C prior to use. By adjusting the feeding ratio of BTZ, TA, and Fe^{3+}, BTZ NPs with different components were obtained by the same method.

In order to investigate if BTZ and TA could form nanoparticles, 500 μL of BTZ solution and 500 μL of TA solution were added into 10 mL ultrapure water. The mixture was stirred for 2 h (800 rpm). After that, the obtained solution was collected and characterized by transmission electron microscopy (TEM) to see if there are nanoparticles in the solution.

In order to investigate if TA and Fe^{3+} could form nanoparticles, 500 μL of TA solution and 5 mg per mL $FeCl_3$ aqueous solution were added into 10 mL ultrapure water. The mixture was stirred for 2 h (800 rpm). After that, the obtained solution was collected and characterized by transmission electron microscopy (TEM) to see if there are nanoparticles in the solution.

2.3 The detection of DLE and DLC

In order to detect the DLE of BTZ NPs, the unencapsulated BTZ was detected by determining the BTZ concentration in the supernatant after centrifugation. The BTZ concentration was measured by reversed-phase high performance liquid chromatography (RP-HPLC).

In order to detect the DLC of BTZ NPs, BTZ NPs solution was lyophilized. 2 mg of BTZ NPs powder was re-dispersed in 20 mL ultrapure water. The solution pH was adjusted to about 3.0 by HCl. After incubating for 24 h to achieve the complete release of BTZ, the BTZ concentration was measured by HPLC.

The DLE and DLC were calculated based on the following equations.

$$\text{DLE}\ (\%) = \frac{\text{weight of loaded BTZ}}{\text{weight of BTZ in feed}} \times 100\%$$

$$\text{DLC}\ (\%) = \frac{\text{weight of loaded BTZ}}{\text{weight of BTZ NPs}} \times 100\%$$

2.4 The storage stability test of BTZ NPs

In order to explore the stability of BTZ NPs during storage at 4 °C, BTZ NPs aqueous solution was photographed at day 0. The hydrodynamic diameter of BTZ NPs was measured at day 0 by dynamic light scattering (DLS). BTZ NPs aqueous solution was then stored at 4 °C. At day 7, the hydrodynamic diameter of BTZ NPs was measured again by DLS. BTZ NPs aqueous solution was again stored at 4 °C. At day 14, BTZ NPs aqueous solution was photographed again, and the hydrodynamic diameter of BTZ NPs was measured by DLS.

2.5 *In vitro* drug release

The release of BTZ from BTZ NPs at different pH values was measured by RP-HPLC. In a typical experiment, 2 mL of BTZ NPs solution (5 mg mL^{-1}) was added to two dialysis bags and then immersed in 20 mL of 10 mM phosphate buffer with pH 5.0 or pH 7.4 in the prepared tubes. The tubes were kept at 37 °C in a constant temperature incubator and continuously shaken (100 rpm). At the designated time intervals, 1 mL of culture medium was taken out and replaced with fresh culture medium. The BTZ concentrations in the collected solution were determined by RP-HPLC. The cumulative release percentage (Er) of BTZ from BTZ NPs was calculated by the following equation

$$\mathrm{Er}\ (\%) = \frac{V_e \sum_{1}^{n-1} C_i + V_0 C_n}{m^{\mathrm{BTZ}}} \times 100\%$$

where V_e is the volume of the supplemented phosphate buffer, V_0 is the whole volume of the release medium, C_i and C_n are the concentration of BTZ, i and n stand for the sample times, and m^{BTZ} is the total amount of BTZ in BTZ NPs.

2.6 Cell culture

The human osteosarcoma cell line Saos-2 cells were cultured in RPMI 1640 containing 10% fetal bovine serum (FBS), 100 mg per mL streptomycin and 100 U per mL penicillin. The human multiple myeloma cell line OPM-2 cells were cultured in IMDM containing 10% FBS and 1% penicillin/streptomycin.

2.7 *In vitro* cytotoxicity experiments

In order to evaluate the cytotoxicity of TA, the conventional CCK-8 assay was adopted. HUVEC cells were inoculated in a 96-well plate at a density of 8000 cells per well. The cells were cultured for 24 h. The culture medium was then replaced with 200 μL fresh culture medium containing different concentrations of TA, with 4 parallel samples in each group, and continued to be cultured for 48 h. The culture medium was then replaced with fresh medium containing CCK-8 (10%) for 1 h. The absorbance of each well at 450 nm was measured by a Bio-Rad microplate reader. The cytotoxicity of TA against Saos-2 cells was also measured by the CCK-8 assay using the same protocol.

The CCK-8 assay was also adopted to evaluate the *in vitro* cytotoxicity of BTZ NPs against cancer cells. Saos-2 cells or OPM-2 cells were inoculated in a 96-well plate at a density of 8000 cells per well. The cells were cultured for 24 h. The culture medium was then replaced with 200 μL fresh culture medium containing different concentrations of free BTZ or BTZ NPs, with 4 parallel samples in each group, and continued to be cultured for 48 h. The culture medium was then replaced with fresh medium containing CCK-8 (10%) for 1 h. The absorbance of each well at 450 nm was measured by a Bio-Rad microplate reader.

2.8 Characterization

The hydrodynamic diameters and zeta potential values of BTZ NPs were measured by dynamic light scattering (DLS) equipment using a Zetasizer Nano-ZS from Malvern Instruments. The morphological images of BTZ NPs were obtained by a transmission electron microscope (TEM) (HT7700, Hitachi). The concentration of BTZ was determined by high-performance liquid chromatography (LC-MS-2020, Shimadzu). The mobile phase was methanol–phosphate buffer (pH 2) 60 : 40. The flow rate was 1 mL min^{-1}. A 254 nm UV detector was used. The X-ray diffraction (XRD) pattern of BTZ NPs was obtained with an X-ray diffractometer (X'Pert Pro MPD, PANalytical). The ultraviolet visible (UV-vis) spectra of BTZ NPs were recorded with a UV-vis spectrophotometer (UV-2700, Shimadzu). Fourier-transform infrared (FT-IR) spectroscopy was performed using an IRTracer-100 spectrometer (Shimadzu). A microplate reader (BioTek, Synergy H1) was used in the CCK-8 assay.

2.9 Statistical analysis

The results were presented as the mean ± standard deviation (SD). Statistical analysis was performed using the GraphPad

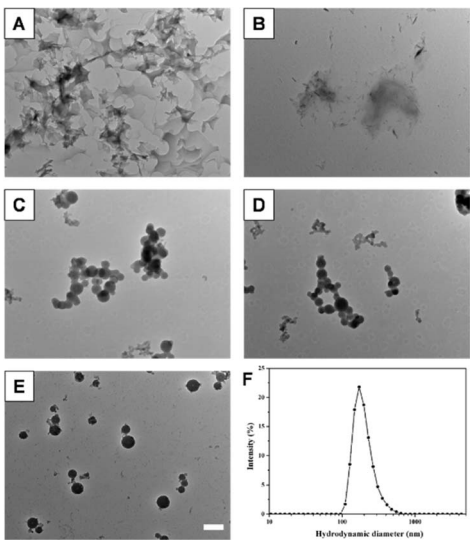

Fig. 1 (A) The TEM image of the compounds after mixing BTZ and TA at a feeding mass ratio of 5 : 16. (B) The TEM image of the compounds after mixing TA and Fe^{3+} at a feeding mass ratio of 48 : 1. (C) The TEM image of BTZ NPs with a feeding mass ratio of BTZ, TA, and Fe^{3+} at 15 : 48 : 1. (D) The TEM image of BTZ NPs with a feeding mass ratio of BTZ, TA, and Fe^{3+} at 75 : 240 : 2. (E) The TEM image of BTZ NPs with a feeding mass ratio of BTZ, TA, and Fe^{3+} at 75 : 240 : 1. Scale bar: 200 nm. (F) The DLS result of BTZ NPs with a feeding mass ratio of BTZ, TA, and Fe^{3+} at 75 : 240 : 1.

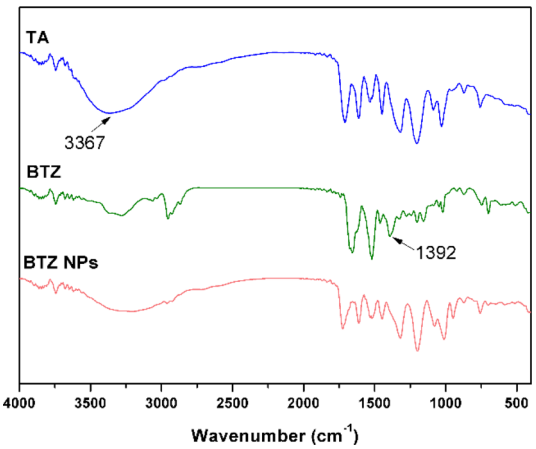

Fig. 2 The FT-IR spectra of TA, BTZ, and BTZ NPs.

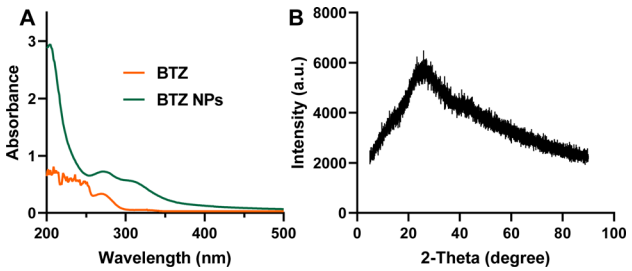

Fig. 3 (A) The UV-vis spectra of BTZ and BTZ NPs with the wavelength from 200 nm to 500 nm. (B) The XRD pattern of BTZ NPs.

Prism or Origin software. An independent-sample *t*-test was used to compare between the two groups. The difference was represented as follows: no significant difference as ns where $p > 0.05$, statistically significant where $*p < 0.05$, and very significant where $**p < 0.01$, $***p < 0.001$, $****p < 0.0001$.

3. Results and discussion

3.1 Preparation of pH-sensitive BTZ NPs

Metal-phenolic networks have attracted much attention owing to their diverse biomedical applications. In particular, metal–polyphenol nanoparticles were prepared by controlling the growth of metal–polyphenol networks. However, metal–polyphenol nanoparticles are seldom used to physically encapsulate the drugs. In order to stably encapsulate drugs into metal–polyphenol nanoparticles, it is necessary that the drug molecules should have specific interaction with metal–polyphenol nanoparticles. It is well-known that boronic acid can bind with diol-containing molecules with high affinity by the formation of reversible boronate ester linkages. Therefore, boronic acid-containing drugs might be encapsulated into metal–polyphenol nanoparticles by the formation of boronate ester bonds between drugs and polyphenols in the nanoparticles. Herein, we tried to encapsulate bortezomib (BTZ) into metal–polyphenol nanoparticles since BTZ is a dipeptide boronic acid analogue.

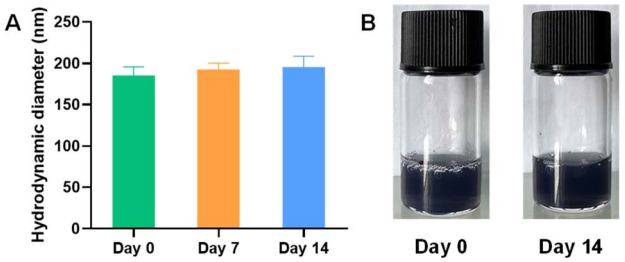

Fig. 4 (A) The hydrodynamic diameters of BTZ NPs in aqueous solution after incubating at 4 °C for 0, 7, and 14 days ($n = 3$). (B) The digital images of BTZ NPs in aqueous solution before and after incubating at 4 °C for 14 days.

In this research, the metal–polyphenol nanoparticles were prepared by the coordination self-assembly between tannic acid (TA) and Fe^{3+}. It should be noted that BTZ-encapsulated TA–Fe capsules were already reported by repeated film deposition on a sacrificial template. Herein, we provided a facile one-pot method to prepare BTZ-encapsulated metal–phenolic nanoparticles.[39] BTZ and Fe^{3+} were unable to self-assemble into nanoparticles since there is only one boronic acid group in one BTZ (Fig. 1A). TA and Fe^{3+} also cannot form nanoparticles (Fig. 1B), which was consistent with previous research. Surprisingly, if BTZ, TA, and Fe^{3+} were added into an aqueous solution together, nanoparticles can be obtained, probably owing to the inhibition of the overgrowth of TA–Fe^{3+} networks by BTZ (Fig. 1C–E). The nanoparticles were prepared by adding BTZ, TA, and $FeCl_3$ into ultrapure water. After stirring for 2 h, nanoparticles were obtained by centrifugation, which could be easily re-dispersed in water. When the feeding mass ratio of BTZ, TA, and Fe^{3+} was 15 : 48 : 1, the obtained nanoparticles did not show satisfactory dispersibility, with a hydrodynamic diameter of 232 nm. The decrease in the Fe^{3+} content could effectively reduce the hydrodynamic diameter and improve the dispersibility of the nanoparticles. If the feeding mass ratio of BTZ, TA, and Fe^{3+} was adjusted to 75 : 240 : 1, well-dispersed BTZ-encapsulated TA–Fe^{3+} nanoparticles (BTZ NPs) were obtained with a hydrodynamic diameter of 185 nm (Fig. 1F), which were used in the following experiments. As shown in the TEM image of BTZ NPs in Fig. 1E, BTZ NPs were spherical with a diameter of about 132 nm. The polydispersity index (PDI) of BTZ NPs was 0.251, which was larger than the diameter determined by TEM, probably owing to the hydration state of BTZ NPs in DLS measurement. The zeta potential of BTZ NPs was −8.5 mV, as detected by DLS. FT-IR was then used to investigate the interaction of BTZ, TA, and Fe^{3+} in BTZ NPs (Fig. 2).[40,41] Compared to the FT-IR spectrum of TA, the signal from phenolic hydroxyl groups at 3367 cm^{-1} was remarkably weakened in the FT-IR spectrum of BTZ NPs, which implied that the phenolic hydroxyl groups of TA formed coordination bond with Fe^{3+}. Meanwhile, the B–O stretching of –B–OH, which was present in the FT-IR spectrum of BTZ, disappeared in the FT-IR spectrum of BTZ NPs, implying the formation of boronate ester bonds in BTZ NPs.

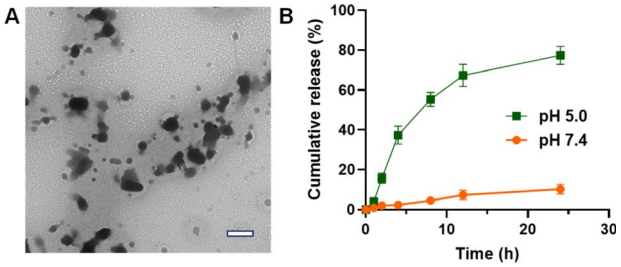

Fig. 5 (A) The TEM image of BTZ NPs after incubating at pH 5.0 for 24 h. Scale bar: 2 μm. (B) The cumulative release of BTZ from BTZ NPs after incubating at pH 7.4 or 5.0 for different time intervals ($n = 3$).

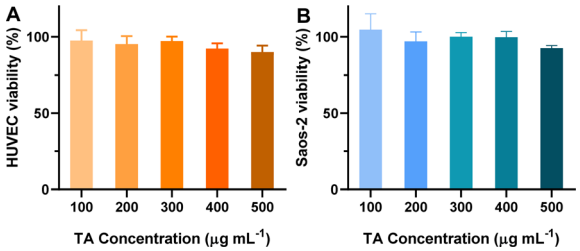

Fig. 6 (A) Cell viability of HUVEC cells incubated with various concentrations of TA for 48 h ($n = 4$). (B) Cell viability of Saos-2 cells incubated with various concentrations of TA for 48 h ($n = 4$).

We further investigated the physiochemical properties of BTZ NPs. The UV-vis spectrum of BTZ NPs is shown in Fig. 3A. The characteristic absorption of BTZ at 275 nm was observed in the UV-vis spectrum of BTZ NPs, which implied that BTZ was successfully encapsulated into TA–Fe^{3+} nanoparticles. XRD was adopted to investigate the crystallinity of BTZ NPs. As shown in Fig. 3B, we did not observe any obvious peaks in the XRD curve, indicating the amorphous structure of BTZ NPs. The drug loading efficiency (DLE) and drug loading content (DLC) of BTZ NPs were detected by measuring the BTZ concentration by HPLC. Due to the strong interaction between BTZ and TA, the DLE of BTZ NPs was as high as 93.4%. Meanwhile, the DLC of BTZ NPs was 21.3%. The storage stability of BTZ NPs was further studied since it was very important for the practical application. As shown in Fig. 4A, we did not observe any aggregation after 14 days' storage. Meanwhile, the size of BTZ NPs did not show an obvious increase, which indicated the excellent storage stability of BTZ NPs (Fig. 4B).

3.2 pH-sensitive drug release

For drug nanodelivery systems, it is critical that the drugs should be effectively released from the nanoparticles. The release of BTZ from BTZ NPs was then investigated. As is known, the dynamic boronate ester bond is pH-sensitive, which could be cleaved in an acidic environment. The coordination interaction between TA and Fe^{3+} is also pH-sensitive, which could be disassembled in an acidic environment. Therefore, after incubating BTZ NPs at pH 5.0 for 2 h, the spherical BTZ NPs were disrupted (Fig. 5A), which was beneficial for the release of BTZ.

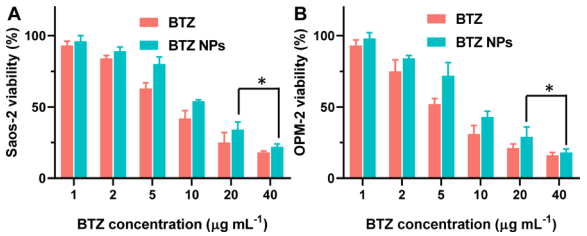

Fig. 7 (A) Cell viability of Saos-2 cells incubated with various concentrations of free BTZ and BTZ NPs for 48 h ($n = 4$). (B) Cell viability of OPM-2 cells incubated with various concentrations of free BTZ and BTZ NPs for 48 h ($n = 4$). Statistical tests were performed using t-test, with p values: $^*p < 0.05$.

The release of BTZ was then investigated by incubating BTZ NPs at different pH values. As shown in Fig. 5B, the release of BTZ from BTZ NPs was very slow at pH 7.4, with only 10% drug release after 24 h incubation. However, the release of BTZ was significantly accelerated in an acidic microenvironment. More than 50% BTZ was released from BTZ NPs after incubating at pH 5.0 for 8 h, which was further increased to 80% after 24 h incubation. The rapid release of BTZ from BTZ NPs in an acidic microenvironment might be ascribed to the disassembly of BTZ NPs as well as the cleavage of pH-sensitive boronate ester bonds. Since BTZ was encapsulated into BTZ NPs by forming dynamic boronate ester bonds, BTZ would be released only when the boronate ester bond between TA and BTZ was cleaved. Therefore, BTZ NPs were stable during blood circulation with minimal drug leakage. However, BTZ could be effectively released from BTZ NPs after internalization by the cancer cells due to the cleavage of dynamic boronate ester bonds in an acidic endo/lysosomal environment. It is very important for enhanced therapeutic efficacy with minimal side effects.

3.3 *In vitro* cytotoxicity

The *in vitro* cytotoxicity of BTZ NPs against cancer cells was investigated by the CCK-8 assay. The human multiple myeloma cell line OPM-2 and human osteosarcoma cell line Saos-2 were used as the model cancer cell lines. Firstly, it is important to study the biocompatibility and safety of the carrier. Unfortunately, the carrier without loading BTZ cannot form nanoparticles. Therefore, we studied the cytotoxicity of TA, which was the main component of the nanocarriers. As shown in Fig. 6A, TA did not show any cytotoxicity against human umbilical vein endothelial cells (HUVEC) when the concentration was as high as 500 μg mL^{-1}, which implied that the blank nanocarrier exhibited excellent biocompatibility. Meanwhile, TA also did not inhibit the proliferation of Saos-2 cells (Fig. 6B).

The inhibition of cancer cell proliferation by BTZ NPs was investigated, and the results are shown in Fig. 7. As shown in Fig. 7A, BTZ NPs and free BTZ exhibited comparable cancer cell inhibition ability against Saos-2 cells. The half inhibitory concentration (IC_{50}) of BTZ in BTZ NPs was 11.3 μg mL^{-1}. When the BTZ equivalent concentration in BTZ NPs was 20 μg mL^{-1}, the cytotoxicity of BTZ NPs against Saos-2 cells did not show significant difference from that of free BTZ. Similarly, BTZ NPs

and free BTZ showed comparable cytotoxicity against OPM-2 cells (Fig. 7B). The IC_{50} of BTZ in BTZ NPs against OPM-2 cells was 8.9 μg mL^{-1}. These results indicated that the encapsulation of BTZ into nanoparticles did not influence the cytotoxicity of BTZ against the cancer cells, probably owing to the efficient release of BTZ from the nanoparticles in an acidic environment.

4. Conclusions

In summary, BTZ-encapsulated TA–Fe^{3+} nanoparticles (BTZ NPs) were successfully prepared by the TA–Fe^{3+} coordination interaction and the formation of dynamic boronate ester bonds. BTZ NPs exhibited spherical and amorphous structures with a hydrodynamic diameter of 185 nm. Owing to the strong interaction among BTZ, TA, and Fe^{3+}, BTZ NPs showed excellent stability in physiological environment (pH 7.4). Therefore, the release of BTZ from BTZ NPs was very slow. However, owing to the disruption of metal–polyphenol networks and cleavage of dynamic boronate ester bonds at acidic pH, BTZ NPs would be disassembled and BTZ could be rapidly released. Furthermore, BTZ NPs exhibited high cytotoxicity against Saos-2 cells and OPM-2 cells, probably owing to the release of BTZ in an acidic endo/lysosomal environment. This research provided a facile and effective strategy to encapsulate BTZ in metal–polyphenol nanoparticles, which might be a very promising nanoplatform to achieve enhanced therapeutic efficacy and reduced side effects of BTZ.

Data availability

The data supporting this article have been included as part of the ESI.†

Author contributions

Haidong Zhou: methodology, investigation, writing-original draft; writing-review & editing, project administration, funding acquisition; Hongyu Xu: validation, formal analysis, writing-review & editing; Jiaping Man: methodology, investigation, visualization; Gangxiang Wang: data curation, software, writing-review & editing.

Conflicts of interest

There are no conflicts to declare.

Acknowledgements

The financial support from Shengzhou People's Hospital is gratefully acknowledged. We thank the equipment and technology service platform, College of Life Science, Zhejiang University for the HPLC measurement.

References

1 R. L. Siegel, A. N. Giaquinto and A. Jemal, *Ca-Cancer J. Clin.*, 2024, **74**, 12–49.
2 V. T. DeVita Jr and E. Chu, *Cancer Res.*, 2008, **68**, 8643–8653.
3 R. C. Kane, P. F. Bross, A. T. Farrell and R. Pazdur, *Oncologist*, 2003, **8**, 508–513.
4 D. Chen, M. Frezza, S. Schmitt, J. Kanwar and Q. P. Dou, *Curr. Cancer Drug Targets*, 2011, **11**, 239–253.
5 D. Chauhan, A. Ray, K. Viktorsson, J. Spira, C. Paba-Prada, N. Munshi, P. Richardson, R. Lewensohn and K. C. Anderson, *Clin. Cancer Res.*, 2013, **19**, 3019.
6 W. Zou, P. Yue, N. Lin, M. He, Z. Zhou, S. Lonial, F. R. Khuri, B. Wang and S.-Y. Sun, *Clin. Cancer Res.*, 2006, **12**, 273.
7 S. Hebballi, J. Muddana, R. Perry, A. Munawwar, A. Shrestha, C. Taylor, C. Arbuthnot and S. W. Bokhari, *Haematol*, 2011, **153**, 48.
8 O. Sartor, *Oncologist*, 2018, **23**, 1.
9 H. Lenz, *Cancer Treat. Rev.*, 2003, **29**, 41.
10 C. N. Papandreou and C. J. Logothetis, *Cancer Res.*, 2004, **64**, 5036.
11 M. J. Nirmala, U. Kizhuveetil, A. Johnson, G. Balaji, R. Nagarajana and V. Muthuvijayan, *RSC Adv.*, 2023, **13**, 8606–8629.
12 H. Son, J. Shin and J. Park, *RSC Adv.*, 2023, **13**, 9788–9799.
13 H. Hu, D. Li, W. Dai, Q. Jin, D. Wang, J. Ji, B. Z. Tang and Z. Tang, *Adv. Funct. Mater.*, 2023, **33**, 2213134.
14 D. Wei, Y. Sun, H. Zhu and Q. Fu, *ACS Nano*, 2023, **17**(23), 23223–23261.
15 P. H. D. Nguyen, M. K. Jayasinghe, A. H. Le, B. Peng and M. T. N. Le, *ACS Nano*, 2023, **17**(6), 5187–5210.
16 V. Gadekar, Y. Borade, S. Kannaujia, K. Rajpoot, N. Anup, V. Tambe, K. Kalia and R. K Tekade, *J. Controlled Release*, 2021, **330**, 372–397.
17 C. Zhang, L. Yan, X. Wang, S. Zhu, C. Chen, Z. Gu and Y. Zhao, *Nano Today*, 2020, **35**, 101008.
18 J. Zhao, W. Dai, L. Zhan, L. Lei, Q. Jin, J. Wang and Z. Tang, *ACS Appl. Mater. Interfaces*, 2024, **16**, 11289–11304.
19 W. Zhang, R. Taheri-Ledari, F. Ganjali, S. S. Mirmohammadi, F. S. Qazi, M. Saeidirad, A. KashtiAray, S. Zarei-Shokat, Y. Tian and A. Maleki, *RSC Adv.*, 2023, **13**, 80–114.
20 J. Xu, S. Chen, J. Yang, Z. Nie, Ju. He, Y. Zhao, X. Liu, J. Zhang and Y. Zhao, *RSC Adv.*, 2023, **13**, 11160–11170.
21 M. Ghezzi, S. Pescina, C. Padula, P. Santi, E. Del Favero, L. Cantù and S. Nicoli, *J. Controlled Release*, 2021, **332**, 312–336.
22 Y. Chen, Y. Luo, S. Chan, W. Chiu and H. Yang, *J. Nanobiotechnol.*, 2023, **21**, 498.
23 F. Yang, Q. Ji, R. Liao, S. Li, Y. Wang, X. Zhang, S. Zhang, H. Zhang, Q. Kan, J. Sun, Z. He, B. Sun and C. Luo, *Chin. Chem. Lett.*, 2022, **33**, 1927–1932.
24 F. Zhao, X. Liu, A. Dong, L. Deng, W. Wang and J. Zhang, *J. Mater. Chem. B*, 2019, **7**, 7490.

25 X. Hu, Z. Chai, L. Lu, H. Ruan, R. Wang, C. Zhan, C. Xie, J. Pan, M. Liu, H. Wang and W. Lu, *Adv. Funct. Mater.*, 2019, **29**, 1807941.
26 G. Gao, Y. Xu, J. Gan, X. Cao, X. Dong, M. Fang, Y. Du, P. Xu, J. Che and B. Chen, *APL Mater.*, 2023, **11**, 121113.
27 D. Dutta, J. Liu, K. Wen, K. Kurata, M. Fulciniti, A. Gulla, T. Hideshima and K. C. Anderson, *Blood Cancer J.*, 2023, **13**, 184.
28 M. Wang, X. Cai, J. Yang, C. Wang, L. Tong, J. Xiao and L. Li, *ACS Appl. Mater. Interfaces*, 2018, **10**, 41003–41011.
29 M. Chen, S. Juengpanich, S. Li, W. Topatana, Z. Lu, Q. Zheng, J. Cao, J. Hu, E. Chan, L. Hou, J. Chen, F. Chen, Y. Liu, S. Jiansirisomboon, Z. Gu, S. Tongpeng and X. Cai, *Adv. Sci.*, 2022, **9**, 2103895.
30 J. D. Ashley, J. F. Stefanick, V. A. Schroeder, M. A. Suckow, T. Kiziltepe and B. Bilgicer, *J. Med. Chem.*, 2014, **57**, 5282–5292.
31 Z. Zhang, L. Xie, Y. Ju and Y. Dai, *Small*, 2021, **17**, 2100314.
32 H. Wang, D. Wang, J. Yu, Y. Zhang and Y. Zhou, *Biomater. Sci.*, 2022, **10**, 5786–5808.
33 Y. Wang, Y. He, Q. Wang, X. Wang, B. L. Tardy, J. J. Richardson, O. J. Rojas and J. Guo, *Matter*, 2023, **6**, 260–273.
34 H. Ejima, J. J. Richardson and F. Caruso, *Nano Today*, 2017, **12**, 136–148.
35 Y. Huang, Y. Chen, Z. Lu, B. Yu, L. Zou, X. Song, H. Han, Q. Jin and J. Ji, *Small*, 2023, **19**, 2302578.
36 J. Gu, P. Zhang, H. Li, Y. Wang, Y. Huang, L. Fan, X. Ma, X. Qian and J. Xi, *ACS Nano*, 2024, **18**, 6229–6242.
37 X. He, H. Zhu, J. Shang, M. Li, Y. Zhang, S. Zhou, G. Gong, Y. He, A. Blocki and J. Guo, *Theranostics*, 2022, **12**, 6258–6272.
38 Y. Huang, Q. Gao, C. Li, X. Chen, X. Li, Y. He, Q. Jin and J. Ji, *Adv. Funct. Mater.*, 2022, **32**, 2109011.
39 Y. Ju, C. Cortez-Jugo, J. Chen, T. Wang, A. J. Mitchell, E. Tsantikos, N. Bertleff-Zieschang, Y. Lin, J. Song, Y. Cheng, S. Mettu, Md. A. Rahim, S. Pan, G. Yun, M. L. Hibbs, L. Y. Yeo, C. E. Hagemeyer and F. Caruso, *Adv. Sci.*, 2020, **7**, 1902650.
40 K. Li, G. Xiao, J. J. Richardson, B. L. Tardy, H. Ejima, W. Huang, J. Guo, X. Liao and B. Shi, *Adv. Sci.*, 2019, **6**, 1801688.
41 Z. Zhou, K. Li, L. Shi, Y. Wang, Y. He, W. Hu and J. Guo, *Adv. Healthcare Mater.*, 2023, **12**, 2201933.